Binary fluid convection in a cylinder

Isabel Mercader and Marta Net
Departament de Física Aplicada, Universitat Politècnica de Catalunya, 08034 Barcelona, Spain

Edgar Knobloch
Department of Physics, University of California, Berkeley, California 94720
(Received 11 July 1994)

The onset of convection in binary fluid mixtures in a vertical cylinder is considered. Parameter values and boundary conditions relevant to experiments on ^{3}He-^{4}He and water-ethanol mixtures with negative separation ratio are used. The azimuthal wave number of the first unstable mode is calculated as a function of the separation ratio, as are the critical Rayleigh numbers and oscillation frequencies. The eigenfunctions take the form of left-handed or right-handed rigidly rotating spirals. Depending on the azimuthal wave number, the spirals may be spatially extended, filling the container, or confined to its boundary. The results are compared with ongoing experiments.

PACS number(s): 47.20.Bp, 47.20.Ky, 47.27.Te, 03.40.Kf

I. INTRODUCTION

Flow visualization has proved to be invaluable in experiments on binary fluid convection in both circular [1] and annular containers [2]. If the annular container is sufficiently narrow the resulting system is approximately two dimensional and much of the observed behavior then agrees with existing theory [3, 4]. Recent experiments in a circular container show, however, that in truly three-dimensional systems new behavior prevails. In particular, Lerman *et al.* [1] show that the initial phase of the instability takes the form of waves that travel radially outwards. These waves do not saturate at finite amplitude and constitute a long-lived transient. The final state is a complicated time-dependent state; no spatially localized stationary three-dimensional patches of convection have yet been found.

The present paper is concerned with the onset of instability in binary fluid mixtures with a negative separation ratio in a vertical nonrotating cylinder. This system is of interest to theorists for several reasons. First, the circular geometry of the container introduces the symmetry O(2) into the dynamical equations. Since for sufficiently negative separation ratios S the onset of instability is oscillatory, the resulting instability is a Hopf bifurcation with O(2) symmetry. When this instability breaks the circular symmetry of the container (i.e., the azimuthal wave number is nonzero) the multiplicity of the imaginary eigenvalue is doubled, and the instability evolves either to a pattern of standing waves or into waves that travel in either direction around the cylinder [5]. This picture is known to describe fully the onset of convection in a narrow annulus. In a large aspect ratio cylinder additional possibilities exist, since waves can also propagate in the radial direction, in spite of the presence of the walls of the cylinder. Indeed, it is well known that traveling waves are present in rectangular containers of sufficiently large aspect ratio [6]. This situation has been studied theoretically by Dangelmayr *et al.* [7], who formulated the problem as a translation invariant problem perturbed by the presence of the sidewalls. The main observation that results is that in a rectangular container the eigenfunctions must take the form of a "chevron" pattern. This pattern has reflection symmetry if identical boundary conditions apply at the sidewalls. In the present case the radial divergence destroys such a reflection symmetry and the problem is properly formulated on the interval $0 < r < \Gamma$. In a sufficiently large aspect ratio cylinder the resulting problem has an approximate symmetry O(2)×SO(2) where the SO(2) symmetry in the radial direction is broken by the walls of the cylinder. It follows that it is possible to find axisymmetric eigenfunctions describing waves traveling in the radial direction, as well as nonaxisymmetric eigenfunctions that travel in addition in the azimuthal direction. Such eigenfunctions naturally take the form of rotating *spirals*. These spirals rotate rigidly, but owing to the walls at the top and bottom of the cylinder they do so with a z-dependent phase, i.e., if we take a fixed r section of the spiral the spiral will be bowed out, with its midlevel either leading or trailing. Which occurs depends sensitively on the parameters of the problem, much as in the two-dimensional problem [8]. Since the theory predicts that in the weakly nonlinear regime both standing (SW) and traveling (TW) waves in the azimuthal direction can be stable we present both SW and TW eigenfunctions, even though at the linear level no selection between different superpositions of clockwise and counterclockwise traveling waves takes place. These states can be either extended, filling the interior of the container, or confined to its boundary. The latter possibility is unexpected since unlike the rotating problem the present system does not support wall modes in the dissipationless regime.

The paper is organized as follows. In Sec. II we formulate the hydrodynamical equations and describe the technique we use to solve them. In Sec. III we describe the results of our computations. Section IV describes the theoretical interpretation of these results. In Sec. V we present results on convective states confined to a straight wall in doubly diffusive convection and relate them to the

results of Sec. III. The final section contains a brief conclusion and comparison with existing experiments.

II. FORMULATION AND METHOD OF SOLUTION

We consider Boussinesq binary fluid convection in a right circular cylinder of height h and radius Γh. The nondimensional equations describing the onset of instability as the Rayleigh number R is increased are given by [8]

$$\frac{1}{\sigma}\partial_t \mathbf{u} = -\nabla p + R(\Theta + S\Sigma)\hat{\mathbf{z}} + \nabla^2 \mathbf{u}, \tag{1a}$$

$$\partial_t \Theta = w + \nabla^2 \Theta, \tag{1b}$$

$$\partial_t \Sigma = w + \tau \nabla^2 \Sigma - \tau \nabla^2 \Theta, \tag{1c}$$

$$\nabla \cdot \mathbf{u} = 0. \tag{1d}$$

Here S is the separation ratio, τ the Lewis number, and σ the Prandtl number. The quantities Θ and Σ denote, respectively, the temperature and concentration perturbations relative to their conduction profiles, while $\mathbf{u} = (u, v, w)$ is the velocity perturbation in cylindrical coordinates (r, ϕ, z). We consider two types of boundary conditions,

$$\frac{\partial u}{\partial z} = \frac{\partial v}{\partial z} = w = \Theta = \frac{\partial \Theta}{\partial z} - \frac{\partial \Sigma}{\partial z} = 0 \text{ on } z = 0, 1, \tag{2a}$$

$$\mathbf{u} = \frac{\partial \Theta}{\partial r} = \frac{\partial \Sigma}{\partial r} = \mathbf{0} \text{ on } r = \Gamma, \tag{2b}$$

and

$$\mathbf{u} = \Theta = \frac{\partial \Theta}{\partial z} - \frac{\partial \Sigma}{\partial z} = \mathbf{0} \text{ on } z = 0, 1, \tag{3a}$$

$$\mathbf{u} = \frac{\partial \Theta}{\partial r} = \frac{\partial \Sigma}{\partial r} = \mathbf{0} \text{ on } r = \Gamma. \tag{3b}$$

Both sets of boundary conditions describe a no-slip no-flux boundary at $r = \Gamma$, with fixed temperature no-mass-flux boundary conditions at the top and bottom, which are stress-free in the former and no-slip in the latter. In the following we refer to these for short as stress-free and rigid. The rigid boundary conditions approximate well the experimental conditions. Note that due to the no-mass-flux boundary conditions at top and bottom the stress-free problem is, like the rigid problem, nonseparable. In the calculations reported below we solve the former using a Galerkin method in the vertical, and the latter using a Chebyshev collocation method. In both cases the collocation method is used in the radial direction [9, 10]. The formulation of the eigenvalue problem is completed by imposing an appropriate regularity condition at $r = 0$ [9].

For positive separation ratios (and hence steady state instabilities) the above problem has been solved by Hardin *et al.* [11]. We focus here on the overstable case present for sufficiently negative separation ratios, and therefore seek solutions of the form $f(r, \phi, z, t) = F(r, z)e^{i(m\phi + \omega t)}$, where $F(r, z)$ depends on the chosen value of m (> 0). The (nonseparable) eigenvalue problem in (r, z) is solved for each m, and yields the critical Rayleigh number $R_c^{(m)}$ and the corresponding Hopf frequency $\omega_c^{(m)}$, for fixed values of τ, σ, S, and Γ. Note that $\omega_c^{(m)} < 0$ for modes that travel counterclockwise, while $\omega_c^{(m)} > 0$ for clockwise modes. By minimizing $R_c^{(m)}$ over m it is possible to identify the azimuthal wave number of the mode that first sets in.

III. RESULTS

In this section we present our results for two aspect ratios, $\Gamma = 2.76$, and $\Gamma = 11.0$. These choices are motivated by ongoing experiments of Lucas and co-workers [12] on ^{3}He-^{4}He mixtures at cryogenic temperatures and by the experiments of Lerman *et al.* [1] on water-ethanol mixtures. These experiments also motivate our choice of the remaining parameters. In Fig. 1 we show (a) the

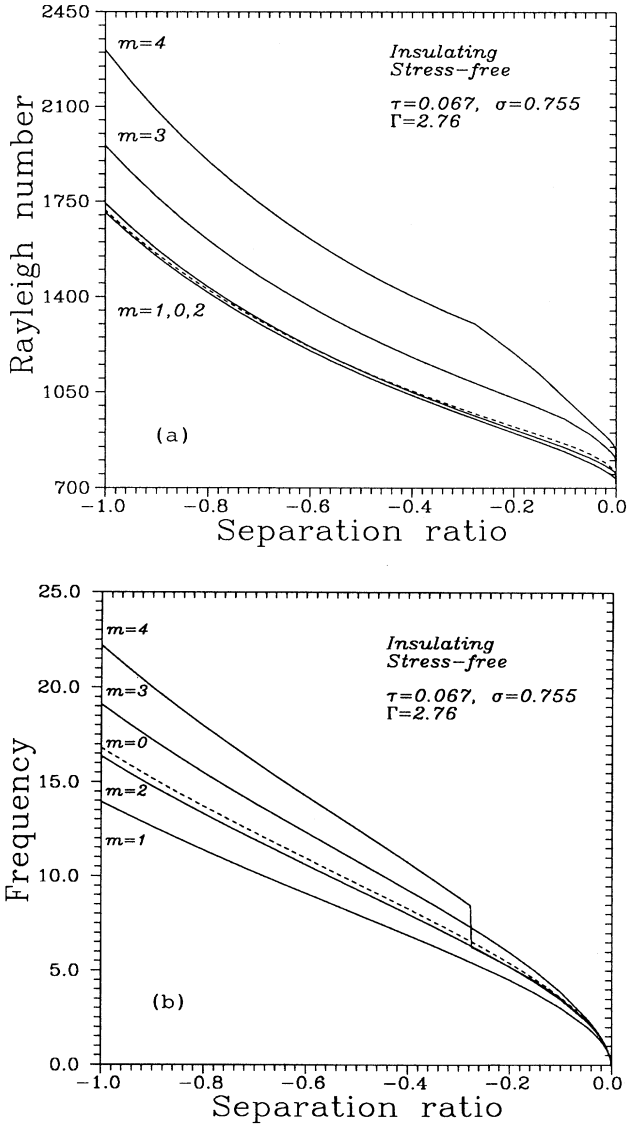

FIG. 1. (a) $R_c^{(m)}(S)$ and (b) $\omega_c^{(m)}(S)$ for $\Gamma = 2.76$, $\tau = 0.067$, $\sigma = 0.755$, and stress-free boundary conditions.

critical Rayleigh numbers $R_c^{(m)}$ and (b) the corresponding frequencies $\omega_c^{(m)}$ as a function of the separation ratio S for $\tau = 0.067$, $\sigma = 0.755$, $\Gamma = 2.76$ and the stress-free boundary conditions (2). For all values of S the selected mode has $m = 1$. Note that the frequencies exhibit discontinuities; these occur when an $m = 1$ mode is superseded by another $m = 1$ mode with a different radial (or vertical) structure. Figure 1 shows only the lowest lying radial modes for each m at each value of S. The $m = 1$ oscillations are present for $S < S_{CT} < 0$. Here $S_{CT} \approx -1.0 \times 10^{-3}$ is the value of S at which oscillations are superseded by a steady state instability [13]. For comparison, Fig. 2 shows the corresponding results for the rigid boundary conditions (3). As before, the mode that is selected in the range $-0.72 < S < S_{CT} \approx -2.3 \times 10^{-3}$ is the $m = 1$ mode; $m = 0$ is preferred for $S < -0.72$. Figure 3 illustrates the sensitive dependence of the results on the assumed parameters: the figure shows the results for rigid boundaries and $\tau = 0.025$, $\sigma = 0.547$. This relatively modest change in the parameters (particularly in τ) results in a significant decrease in the critical Rayleigh numbers even though throughout most of the range the selected wave number remains unchanged: the transition from $m = 1$ to $m = 0$ now takes place when $S = -0.74$.

In Fig. 4 we illustrate the eigenfunctions for the $m = 1$ mode at $R = R_c^{(1)}$, $S = -0.288$, corresponding to Fig. 2. Figure 4(a) shows the temperature eigenfunction $\mathrm{Re}\Theta(r,z)e^{i(m\phi+\omega t)}$ at $z = \frac{1}{2}$ in the comoving frame as a function of r and ϕ using two different representa-

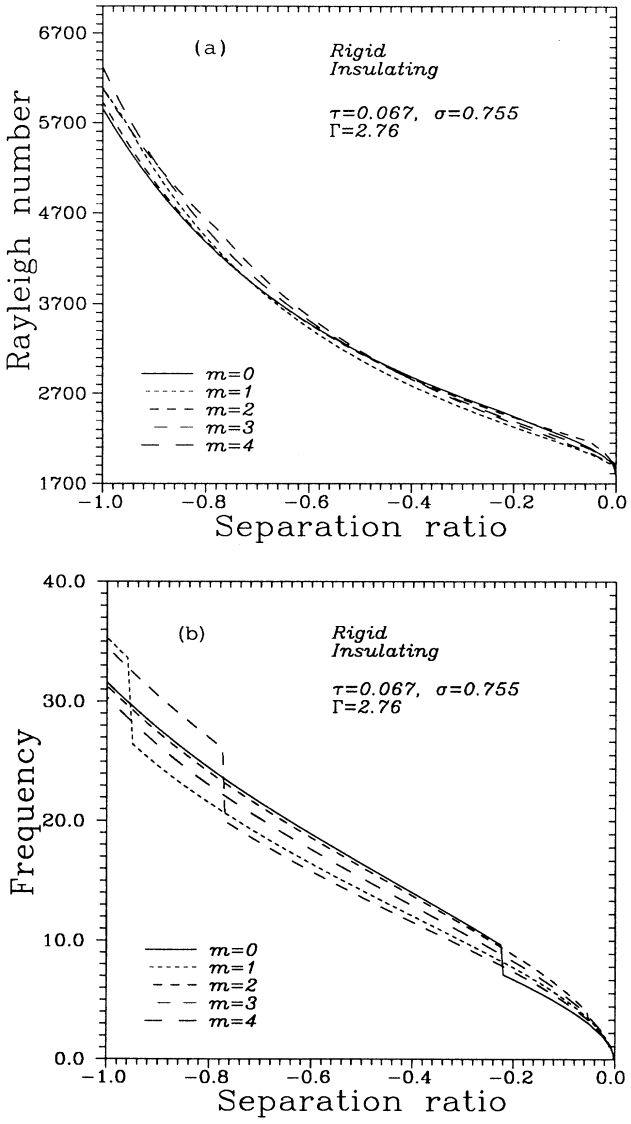

FIG. 2. (a) $R_c^{(m)}(S)$ and (b) $\omega_c^{(m)}(S)$ for $\Gamma = 2.76$, $\tau = 0.067$, $\sigma = 0.755$, and rigid boundary conditions.

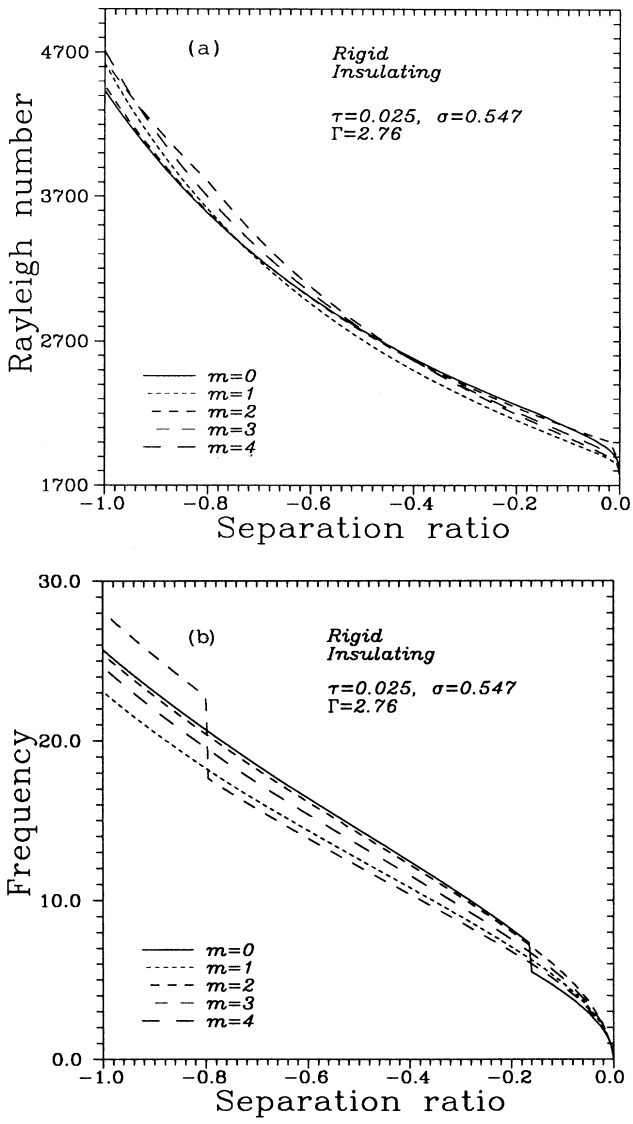

FIG. 3. (a) $R_c^{(m)}(S)$ and (b) $\omega_c^{(m)}(S)$ for $\Gamma = 2.76$, $\tau = 0.025$, $\sigma = 0.547$, and rigid boundary conditions.

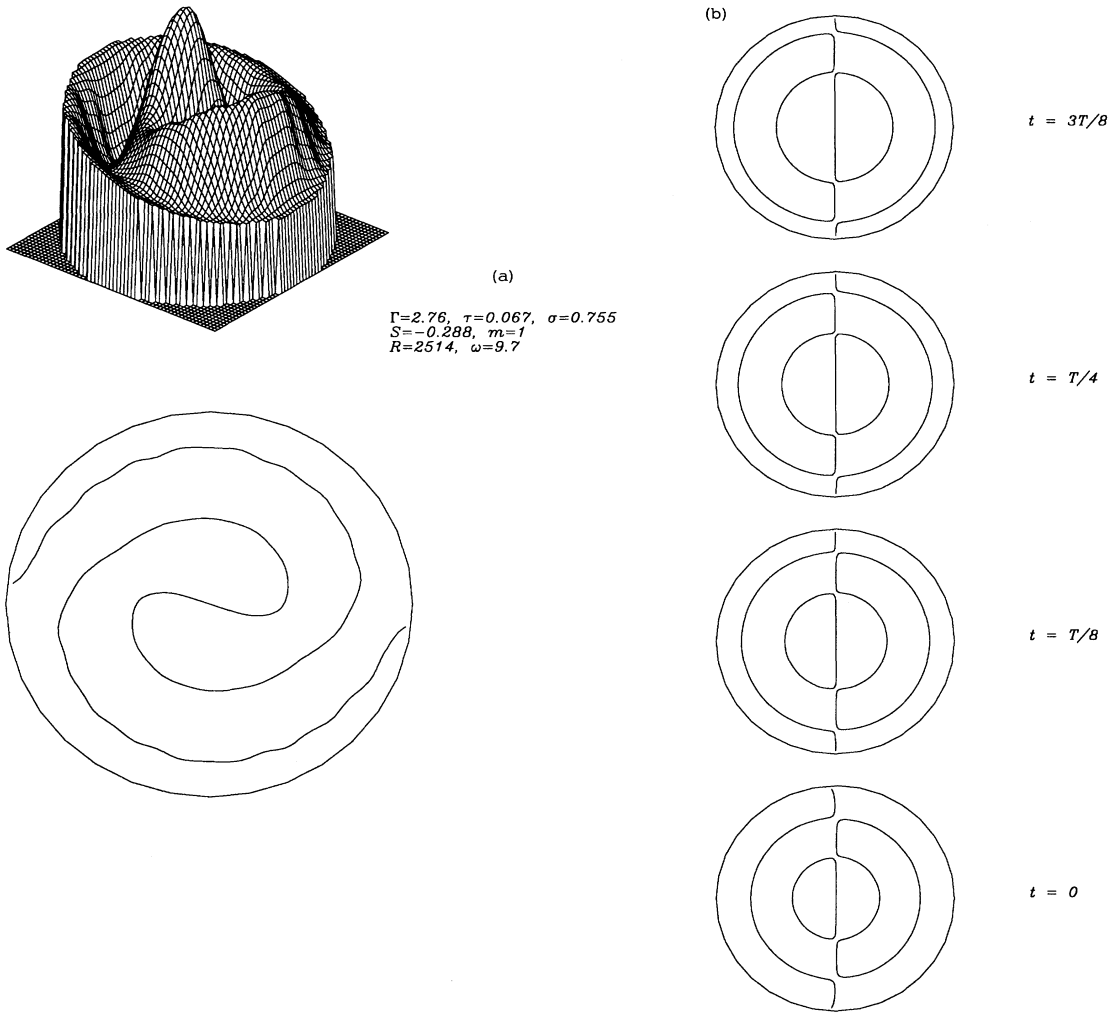

FIG. 4. (a) The temperature eigenfunction $\Theta(r, \phi, z = \frac{1}{2})$ for an $m = 1$ TW mode at $R = R_c^{(1)} \equiv 2514$, for $\Gamma = 2.76$, $\tau = 0.067$, $\sigma = 0.755$, $S = -0.288$, and rigid boundary conditions. The precession frequency is $\omega_c^{(1)} = 9.7$. (b) The corresponding SW eigenfunction at $t = 0, \frac{T}{8}, \frac{T}{4}, \frac{3T}{8}$, where $T \equiv 2\pi/\omega_c^{(1)}$ is the oscillation period. Note that the mode peaks near both the center and the walls of the container.

tions. The eigenfunction peaks both near the wall and near the center; the whole pattern rotates rigidly in the clockwise direction. Owing to the reflection symmetry in O(2) there is a corresponding solution with the opposite handedness that rotates in the counterclockwise direction. Figure 4(b) shows the SW eigenfunction constructed from these two eigenfunctions. The figure shows contours of constant temperature at four equally spaced times within half an oscillation period. Figure 5 shows the corresponding results for $m = 7$. Although this mode is not the first to set in ($R_c^{(7)} = 3299$) it illustrates an important property of these modes. With increasing m the spirals become less pronounced and more and more confined to the wall, although they continue to rotate with their arms trailing. Figure 5 is important because it reveals that modes that look like the wall modes recently found in pure fluid convection in a *rotating* cylinder [10, 14, 15] can appear even in a nonrotating cylinder.

A vertical section at fixed r shows that both the $m = 1$ and the $m = 7$ waves shown in Fig. 4 lead at midlevel with the points near $z = 0, 1$ trailing behind. The resulting curvature depends both on r and on the system parameters. This is because the eigenfunction can be written in the form

$$\mathrm{Re}\Theta(r, z)e^{i(m\phi+\omega t)} = |\Theta(r, z)| \cos[m\phi + \omega t + \Phi(rz)]. \tag{4}$$

The phase $\Phi(r, z)$ differs for the different fields Θ, Σ, u, v, and w and it is these phase lags that are responsible for

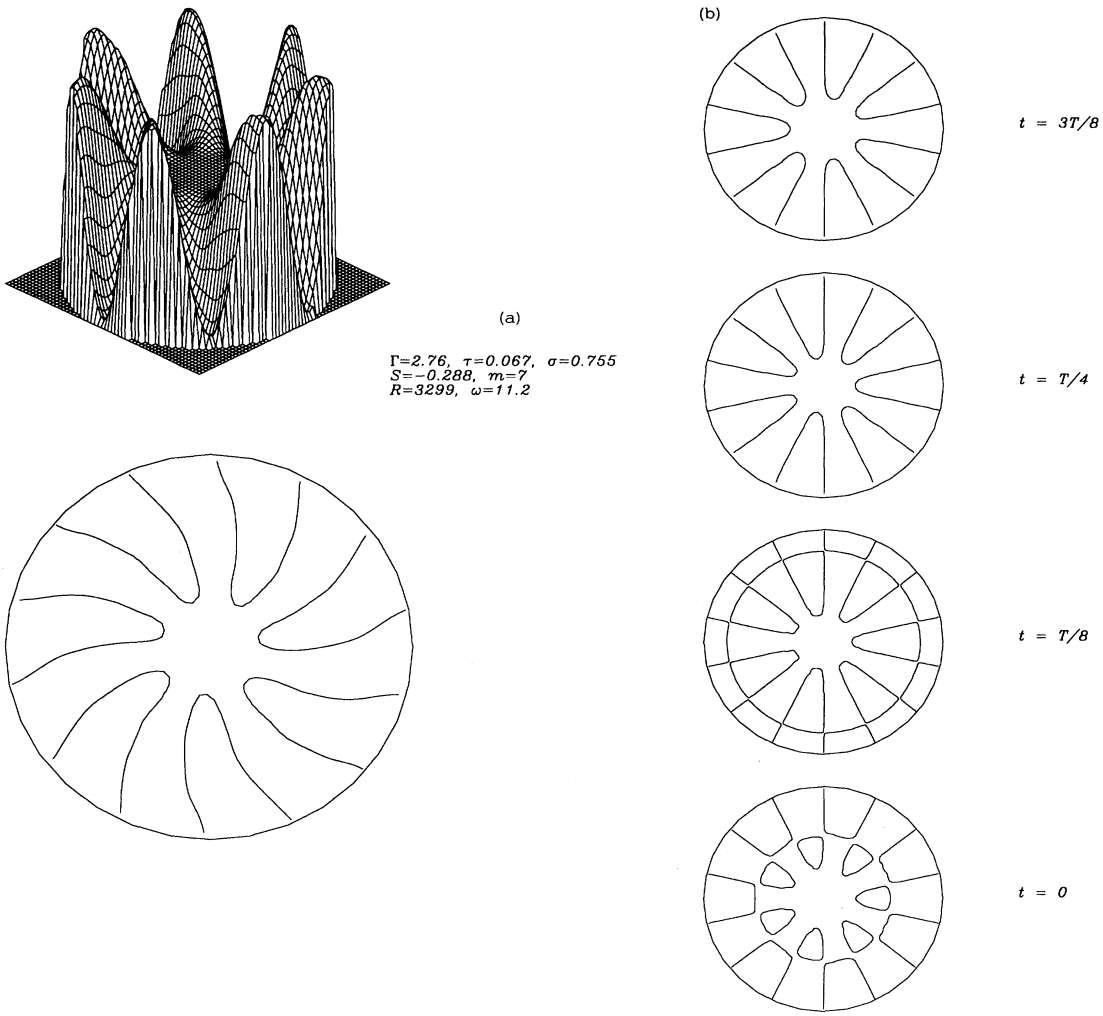

FIG. 5. As for Fig. 4 but for $m = 7$, $R_c^{(7)} = 3299$, and $\omega_c^{(7)} = 11.2$. (a) TW; (b) SW. Note that the mode is now confined to the wall of the container.

the propagation of the wave (cf. [16, 17]). Similar behavior is present already in the two-dimensional plane layer as soon as realistic boundary conditions are imposed at the top and bottom [8]. In contrast, a SW eigenfunction can be written in the form

$$\mathrm{Re}\Theta(r,z)e^{i\omega t}\cos m\phi = |\Theta(r,z)|\cos m\phi\cos[\omega t + \Phi(r,z)]. \tag{5}$$

Such a wave does not propagate in ϕ, but typically does in r.

In general a mode of the form (4) propagates in *both* the azimuthal and radial directions, and takes the form of a rigidly rotating *spiral*. This is illustrated in Fig. 6 for an $m = 1$ mode in a larger aspect ratio cylinder, $\Gamma = 11.0$, with $\tau = 0.008$, $\sigma = 24.0$, $S = -0.09$, and rigid boundary conditions. Figure 6(a) shows the $z = \frac{1}{2}$ section of the resulting spiral in the (r,ϕ) plane. The spiral rotates in the *clockwise* direction so that each point in this plane experiences a pattern of locally parallel rolls drifting radially outwards. This time dependence is shown more explicitly in Fig. 6(b), which shows the corresponding SW eigenfunction (5) in the (r,t) plane, $-\Gamma < r < \Gamma$. The figure reveals that the wave travels outwards towards the boundary, as expected from the observation that it is a superposition of two spirals that rotate in opposite directions. In contrast, for stress-free boundaries and $\Gamma = 11.6$, $\tau = 0.0076$, $\sigma = 23.86$, it is the $m = 0$ mode that is preferred for $S < -0.07$ with $m = 2$ preferred for $-0.07 < S < -0.04$ and again for $-0.85 \times 10^{-5} < S < S_{CT} \approx -0.82 \times 10^{-5}$, with $m = 4$ preferred in between.

IV. THEORETICAL INTERPRETATION

In this section we try to understand the origin of the unstable modes computed numerically in the preceding

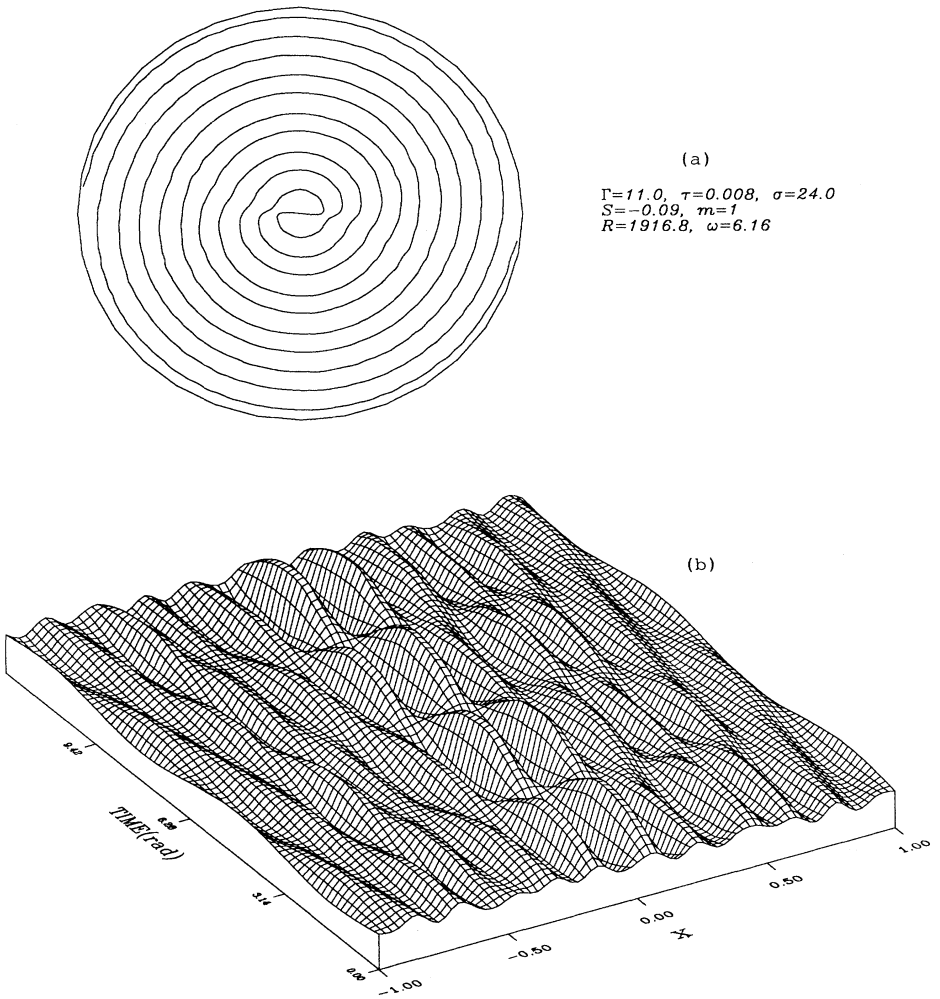

FIG. 6. (a) Contour plot of $\Theta(r, \phi, z = \frac{1}{2})$ for an $m = 1$ TW mode with rigid boundary conditions in a larger aspect ratio container, $\Gamma = 11.0$, $\tau = 0.008$, $\sigma = 24.0$, and $S = -0.09$. Here $R_c^{(1)} = 1916.8$ and $\omega_c^{(1)} = 6.16$. (b) The corresponding SW mode in the (x, t) plane, where $x = r/\Gamma$. The wave travels outwards from the center of the container at $x = 0$.

section. In particular we are interested in elucidating the origin of the modes that look like the wall modes described earlier for convection in a pure fluid but in a rotating cylinder. We begin by showing that the dissipationless problem has no neutrally stable wall modes. Consequently the computed wall modes must be produced as a result of dissipation and thermal forcing. We then discuss this process, following [18, 19], using a simplified model consisting of a fluid-filled semi-infinite domain bounded by a straight boundary, and use this model to identify semianalytically modes of the type shown in Fig. 5.

A. The dissipationless problem

We begin by considering the dissipationless system. We suppose that there are two competing contributions to the density stratification, arising from, say, thermal and solutal stratification. These affect the density in opposite ways, but in the absence of dissipation no diffusive instabilities can take place. Consequently, the dynamics of the system are described by the overall density distribution which we take to be statically stable (density decreasing upwards). The overall density stratification is measured by the Brunt-Väisälä frequency $N \equiv \{-\frac{g}{\rho}\frac{d\rho}{dz}\}^{1/2}$, assumed to be positive. The natural time scale for the neutrally stable oscillations is then N^{-1} with velocities expressed in units of hN, where h is the height of the cylinder. The nondimensional equations take the form

$$\partial_t \mathbf{u} = -\nabla p + \frac{1}{N^2}(N_T^2\Theta - N_S^2\Sigma)\hat{\mathbf{z}}, \tag{6a}$$

$$\partial_t \Theta = w, \tag{6b}$$

$$\partial_t \Sigma = w, \tag{6c}$$

$$\nabla \cdot \mathbf{u} = 0, \tag{6d}$$

where $N_T^2 = -g\alpha\frac{\partial T_0}{\partial z}$, $N_S^2 = -g\beta\frac{\partial S_0}{\partial z}$, and T_0 and S_0 are the (linear) temperature and concentration profiles in the basic state. Both T_0 and S_0 are assumed to decrease with height so that $N_T^2 > 0$, $N_S^2 > 0$. We look for infinitesimal oscillations with dimensionless frequency ω/N. The frequency ω is an eigenvalue of the problem

$$\nabla^2 w + \frac{N^2}{\omega^2 - N^2}\frac{\partial^2 w}{\partial z^2} = 0 \tag{7}$$

specified by the boundary conditions $\mathbf{u}\cdot\mathbf{n} = 0$ on the boundaries of the cylinder. Here $N^2 \equiv N_S^2 - N_T^2$ and $\mathbf{n}$ is the outward normal to the surface. These boundary conditions correspond to stress-free fixed temperature and concentration boundary conditions at the top and bottom, with stress-free no-flux boundary conditions on the sides. These boundary conditions are the only ones compatible with the absence of dissipation. The resulting eigenvalue problem is separable, and we seek solutions of the form $w(r,\phi,z) = W(r)e^{im\phi}\sin n\pi z$, where $W(r)$ satisfies

$$\frac{1}{r}\frac{d}{dr}r\frac{dW}{dr} - \frac{m^2}{r^2}W - \frac{\omega^2}{\omega^2 - N^2}n^2\pi^2 W = 0, \quad n > 0, \tag{8}$$

$$W(0) = 0, W'(\Gamma) = 0. \tag{9}$$

For $m = 0$ the first condition is replaced by $W'(0) = 0$. It follows that

$$W(r) = J_m(\alpha r), \tag{10}$$

where

$$\alpha^2 \equiv \frac{n^2\pi^2\omega^2}{N^2 - \omega^2}, \tag{11}$$

and α_{km} $(k = 1, 2, ...)$ are the roots of $J_m'(\alpha\Gamma) = 0$ and are real. Consequently, for each pair (m,n) there is a discrete unbounded sequence of eigenfrequencies $|\omega_1| < |\omega_2| < \cdots$. Since ω appears only as a square both positive and negative frequencies are allowed. The corresponding eigenfunctions are of class I in the terminology of Friedlander and Siegmann [20] and are oscillatory in r. There are no class II eigenmodes of the form $I_m(|\alpha|r)$. Such modes correspond to wall modes and are only present in stratified systems in the presence of rotation [20]. Their absence implies that no true wall modes will be present in the system under study.

B. The limit of weak dissipation

We can easily determine the effect of small dissipation on the modes identified above. We write the equations in the dimensionless form

$$\partial_t \mathbf{u} = -\nabla p + \frac{1}{N^2}(N_T^2\Theta - N_S^2\Sigma)\hat{\mathbf{z}} + \sigma E\nabla^2\mathbf{u}, \tag{12a}$$

$$\partial_t\Theta = w + E\nabla^2\Theta, \tag{12b}$$

$$\partial_t\Sigma = w + \tau E\nabla^2\Sigma, \tag{12c}$$

$$\nabla\cdot\mathbf{u} = 0, \tag{12d}$$

where $E \equiv \frac{\kappa}{Nh^2}$ is the dimensionless measure of the importance of thermal diffusion, and time is measured in units of N^{-1}, as before. We look for solutions of the form e^{st}, with the growth rate s satisfying the eigenvalue problem

$$(s - \sigma E\nabla^2)(s - E\nabla^2)(s - \tau E\nabla^2)\nabla^2 w$$

$$= \frac{1}{N^2}[N_T^2(s - \tau E\nabla^2) - N_S^2(s - E\nabla^2)]\nabla_\perp^2 w, \tag{13}$$

where $\nabla_\perp^2$ denotes the horizontal Laplacian. As boundary conditions we continue to use the boundary conditions employed in the dissipationless case. While not essential, this choice does provide a considerable simplification in that diffusive boundary layers are avoided. The boundary conditions are thus

$$\frac{\partial}{\partial z}\mathbf{u}_\perp = w = \Theta = \Sigma = 0 \text{ on } z = 0, 1, \tag{14a}$$

$$\mathbf{u}\cdot\mathbf{n} = \frac{\partial w}{\partial r} = \frac{\partial\Theta}{\partial r} = \frac{\partial\Sigma}{\partial r} = 0 \text{ on } r = \Gamma, \tag{14b}$$

with regularity conditions imposed at $r = 0$. Note that these boundary conditions are independent of E.

The resulting eigenvalue problem is easily solved in powers of E. Let

$$w = w_0 - iE\frac{N}{\omega_0}w_1 + \cdots, s = i\frac{\omega_0}{N} + Es_1 + \cdots. \tag{15}$$

Then at $O(E^0)$ one recovers the solution to the dissipationless problem, with w_0 and ω_0 satisfying (10) and (11), respectively. At $O(E^1)$ one obtains

$$[-\omega_0^2\nabla^2 + N^2\nabla_\perp^2]w_1 = (N_S^2 - \tau N_T^2)\nabla_\perp^2\nabla^2 w_0 - \omega_0^2\Delta\nabla^4 w_0 + s_1(3\omega_0^2\nabla^2 w_0 - N^2\nabla_\perp^2 w_0), \tag{16}$$

where $\Delta \equiv 1 + \sigma + \tau$. It follows that $w_1 = W_1(r)e^{im\phi}\sin n\pi z$. The solvability condition for the radial dependence yields an expression for the dimensionless growth rate s_1. This can be simplified using the relations

$$(\omega_0^2 - N^2)\nabla^2 w_0 = N^2 n^2\pi^2 w_0,$$

$$(\omega_0^2 - N^2)\nabla_\perp^2 w_0 = \omega_0^2 n^2\pi^2 w_0 \tag{17}$$

obtained from the $O(E^0)$ problem. Canceling $\int_0^\Gamma r J_m^2(\alpha r)dr$ from both sides one obtains

$$s_1 = \frac{n^2\pi^2}{2(N^2 - \omega_0^2)}\left[(1+\sigma)N_T^2 - (\sigma+\tau)N_S^2\right], \quad N^2 - \omega_0^2 > 0. \tag{18}$$

It follows that neutrally stable oscillations occur when N_T^2 reaches the value

$$N_{Tc}^2 \equiv \frac{\sigma + \tau}{1 + \sigma}N_S^2 < N_S^2. \tag{19}$$

Consequently, instability sets in at a lower value of the destabilizing temperature gradient than in the dissipationless problem. This is the hallmark of all doubly diffusive systems. Note that there is no N_S-independent term in N_{Tc}^2. This term is $O(E^2)$ and so is absent in the limit $E \ll 1$. Consequently there is no mode selection in this limit. These results are thus in complete agreement with those for an unbounded layer [21]. This is because our choice of boundary conditions eliminated all surface terms from the solvability condition and allowed the cancellation of the integrals.

It is easy to check that a similar analysis of Eqs. (1) leads to the same conclusion. In particular, one finds

that the unstable modes are all of class I and hence fill the body of the container. The perturbation technique is thus not able to identify modes of the type exhibited in Fig. 5.

V. WALL MODES DUE TO A STRAIGHT BOUNDARY

In this section we consider a simplified form of the linear eigenvalue problem in a cylinder. Specifically we consider oscillations in a semi-infinite domain $\{-\infty < x < 0, 0 < z < 1\}$ with a no-slip boundary placed at $x = 0$ and free-slip boundaries at $z = 0, 1$. For comparison with Sec. IV we consider doubly diffusive convection with boundary conditions on the temperature and concentration that are no flux at the sidewall and fixed temperature and concentration at $z = 0, 1$. These boundary conditions are chosen to render the resulting eigenvalue problem separable. Moreover, with these boundary conditions the doubly diffusive problem can be mapped by a linear transformation onto the corresponding Soret-driven problem [22]. Consequently, if there are wall-confined solutions to the doubly diffusive problem, such solutions also exist for the Soret problem. For these modes all fields are assumed to vanish exponentially as $x \to -\infty$. Since we now consider dissipation that can be large enough that $E = O(1)$ we employ instead the thermal diffusion time in the vertical as the unit of time. The problem is then described by the nondimensional equations

$$\frac{1}{\sigma}\partial_t \mathbf{u} = -\nabla p + (R_T\Theta - R_S\Sigma)\hat{\mathbf{z}} + \nabla^2\mathbf{u}, \tag{20a}$$

$$\partial_t\Theta = w + \nabla^2\Theta, \tag{20b}$$

$$\partial_t\Sigma = w + \tau\nabla^2\Sigma, \tag{20c}$$

$$\nabla\cdot\mathbf{u} = 0, \tag{20d}$$

where R_T and R_S are the usual thermal and solutal Rayleigh numbers. We look for solutions of the form $f(x,z)e^{i(my+\omega t)}$, where m is now a continous wave number ($m \neq 0$). With the boundary conditions chosen the problem is separable in z and hence

$$(u, v, w, \Theta, \Sigma, p) = (U(x)\cos\pi z, V(x)\cos\pi z, W(x)\sin\pi z, \Theta(x)\sin\pi z, \Sigma(x)\sin\pi z, P(x)\cos\pi z),$$

where

$$\frac{i\omega}{\sigma}U = -DP + (D^2 - \pi^2 - m^2)U, \tag{21a}$$

$$\frac{i\omega}{\sigma}V = -imP + (D^2 - \pi^2 - m^2)V, \tag{21b}$$

$$\frac{i\omega}{\sigma}W = \pi P + R_T\Theta - R_S\Sigma + (D^2 - \pi^2 - m^2)W, \tag{21c}$$

$$i\omega\Theta = W + (D^2 - \pi^2 - m^2)\Theta, \tag{21d}$$

$$i\omega\Sigma = W + \tau(D^2 - \pi^2 - m^2)\Sigma, \tag{21e}$$

$$DU + \pi W = -imV. \tag{21f}$$

It follows that

$$\left(D^2 - \pi^2 - m^2 - \frac{i\omega}{\sigma}\right)[(D^2 - m^2)U + \pi DW] = 0 \tag{22a}$$

$$\left(D^2 - \pi^2 - m^2 - \frac{i\omega}{\sigma}\right)[(D^2 - m^2)V + im\pi W] = 0, \tag{22b}$$

where

$$(D^2 - \pi^2 - m^2)\left(D^2 - \pi^2 - m^2 - \frac{i\omega}{\sigma}\right)(D^2 - \pi^2 - m^2 - i\omega)\left(D^2 - \pi^2 - m^2 - \frac{i\omega}{\tau}\right)W$$
$$- R_T\left(D^2 - \pi^2 - m^2 - \frac{i\omega}{\tau}\right)(D^2 - m^2)W + \frac{R_S}{\tau}(D^2 - \pi^2 - m^2 - i\omega)(D^2 - m^2)W = 0, \tag{23}$$

subject to the boundary conditions

$$U = V = W = D\Theta = D\Sigma = 0 \text{ on } x = 0 \tag{24}$$

and the requirement that the solutions vanish exponentially as $x \to -\infty$.

To find such solutions we suppose that $W(x) = e^{\lambda x}$ with $\mathrm{Re}\lambda > 0$. It follows that

$$W(x) = \sum_{j=1}^{4} A_j e^{\lambda_j x}, \tag{25}$$

where $\lambda_j^2 \equiv q_j + \pi^2 + m^2$ and the q_j are the roots of the quartic

$$q\left(q - \frac{i\omega}{\sigma}\right)(q - i\omega)\left(q - \frac{i\omega}{\tau}\right) - R_T\left(q - \frac{i\omega}{\tau}\right)(q + \pi^2)$$
$$+ \frac{R_S}{\tau}(q - i\omega)(q + \pi^2) = 0. \tag{26}$$

The corresponding expressions for the remaining fields are readily found from Eqs. (21):

$$U(x) = -\pi\sum_{j=1}^{4} A_j \frac{\lambda_j}{\lambda_j^2 - m^2}e^{\lambda_j x} - imA_5 e^{\mu x}, \tag{27a}$$

$$V(x) = -im\pi \sum_{j=1}^{4} A_j \frac{1}{\lambda_j^2 - m^2} e^{\lambda_j x} + A_5 \mu e^{\mu x}, \tag{27b}$$

$$D\Theta(x) = -\sum_{j=1}^{4} A_j \frac{\lambda_j}{\lambda_j^2 - m^2 - \pi^2 - i\omega} e^{\lambda_j x}, \tag{27c}$$

$$D\Sigma(x) = -\frac{1}{\tau} \sum_{j=1}^{4} A_j \frac{\lambda_j}{\lambda_j^2 - m^2 - \pi^2 - \frac{i\omega}{\tau}} e^{\lambda_j x}, \tag{27d}$$

where

$$\mu^2 = \pi^2 + m^2 + \frac{i\omega}{\sigma}, \quad \mu > 0. \tag{28}$$

The five unknowns A_1, A_2, A_3, A_4, and A_5 are determined by the five boundary conditions imposed at $x = 0$. A nontrivial solution exists if and only if a certain 5×5 determinant vanishes. This requirement yields a complex equation for the critical Rayleigh number $R_T(m)$ and the corresponding frequency $\omega(m)$ of the oscillations.

This determinant takes the form

$$\det \begin{pmatrix} 1 & 1 & 1 & 1 & 0 \\ \frac{\lambda_1}{\lambda_1^2-m^2} & \frac{\lambda_2}{\lambda_2^2-m^2} & \frac{\lambda_3}{\lambda_3^2-m^2} & \frac{\lambda_4}{\lambda_4^2-m^2} & m^2 \\ \frac{1}{\lambda_1^2-m^2} & \frac{1}{\lambda_2^2-m^2} & \frac{1}{\lambda_3^2-m^2} & \frac{1}{\lambda_4^2-m^2} & \mu \\ \frac{\lambda_1}{\lambda_1^2-m^2-\pi^2-i\omega} & \frac{\lambda_2}{\lambda_2^2-m^2-\pi^2-i\omega} & \frac{\lambda_3}{\lambda_3^2-m^2-\pi^2-i\omega} & \frac{\lambda_4}{\lambda_4^2-m^2-\pi^2-i\omega} & 0 \\ \frac{\lambda_1}{\lambda_1^2-m^2-\pi^2-i\omega/\tau} & \frac{\lambda_2}{\lambda_2^2-m^2-\pi^2-i\omega/\tau} & \frac{\lambda_3}{\lambda_3^2-m^2-\pi^2-i\omega/\tau} & \frac{\lambda_4}{\lambda_4^2-m^2-\pi^2-i\omega/\tau} & 0 \end{pmatrix} = 0, \tag{29}$$

and reduces to that for the onset of steady convection when $\omega = 0$; it can also be used to compute the growth rates for supercritical values of R_T by replacing $i\omega$ by $s+i\omega$, where s is the growth rate. Minimization of $R_T(m)$ with respect to m determines R_{Tc} and ω_c, as well as m_c. If the overstable critical Rayleigh number R_{Tc}^{Hopf} is less than the stationary Rayleigh number R_{Tc}^{SS} convection is overstable; otherwise it is steady.

The results of solving Eq. (29) are shown in Fig. 7, which shows the vertical velocity eigenfunction as a function of x at fixed y, z, and t for $m = 1, 2$ and (a) $\tau = 0.067$, $\sigma = 0.755$, $R_S = 750$, and (b) $\tau = 0.316$, $\sigma = 1.0$, $R_S = 1000$. The corresponding critical Rayleigh numbers and frequencies are (a) $R_{Tc}^{(1)} = 2023.10$, $\omega_c^{(1)} = 5.23$, $R_{Tc}^{(2)} = 1338.44$, $\omega_c^{(2)} = 10.09$, and (b) $R_{Tc}^{(1)} = 3049.49$, $\omega_c^{(1)} = 4.44$; $R_{Tc}^{(2)} = 2009.19$, $\omega_c^{(2)} = 9.74$. Observe that in both cases the eigenfunction is confined to the vicinity of the wall ($x = 0$) and decays exponentially away from the wall ($x \to -\infty$). We will call such confined solutions wall modes, by analogy with the rotating Bénard problem. In contrast to the rotating problem, however, the wall modes in the present problem exist only for a limited range of m, $m_c^- < m < m_c^+$. As m approaches $m_c^\pm$ from inside this interval the decay length of the eigenfunction diverges, i.e., Eq. (26) has an eigenvalue λ with $\text{Re}\lambda = 0$. In Fig. 8(a) we show m_c^+ as a function of R_S for $\tau = 0.067$, $\sigma = 0.755$. Figures 8(b) and 8(c) show the corresponding R_{Tc} and ω_c for $m_c^- < m < m_c^+$ when $R_S = 750$ and 4000. Observe that m_c^+ first increases with R_S before decreasing again. However, R_{Tc} and ω_c at this

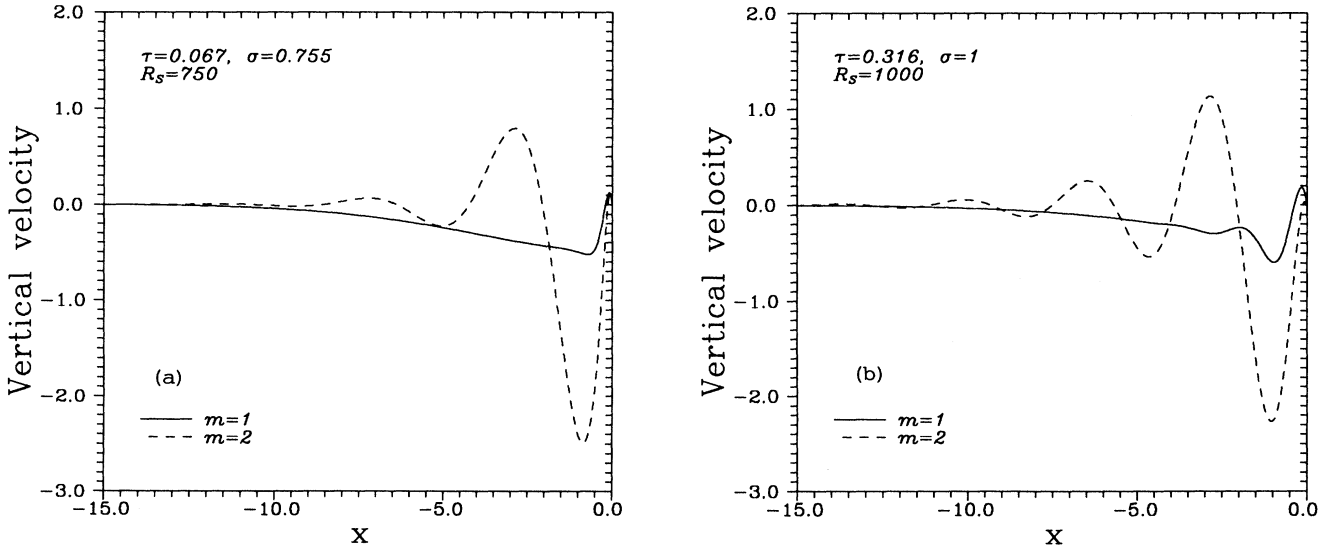

FIG. 7. Vertical velocity eigenfunction near the wall ($x = 0$) for wall modes with $m = 1, 2$ and (a) $\tau = 0.067$, $\sigma = 0.755$, $R_S = 750$, (b) $\tau = 0.316$, $\sigma = 1.0$, $R_S = 1000$.

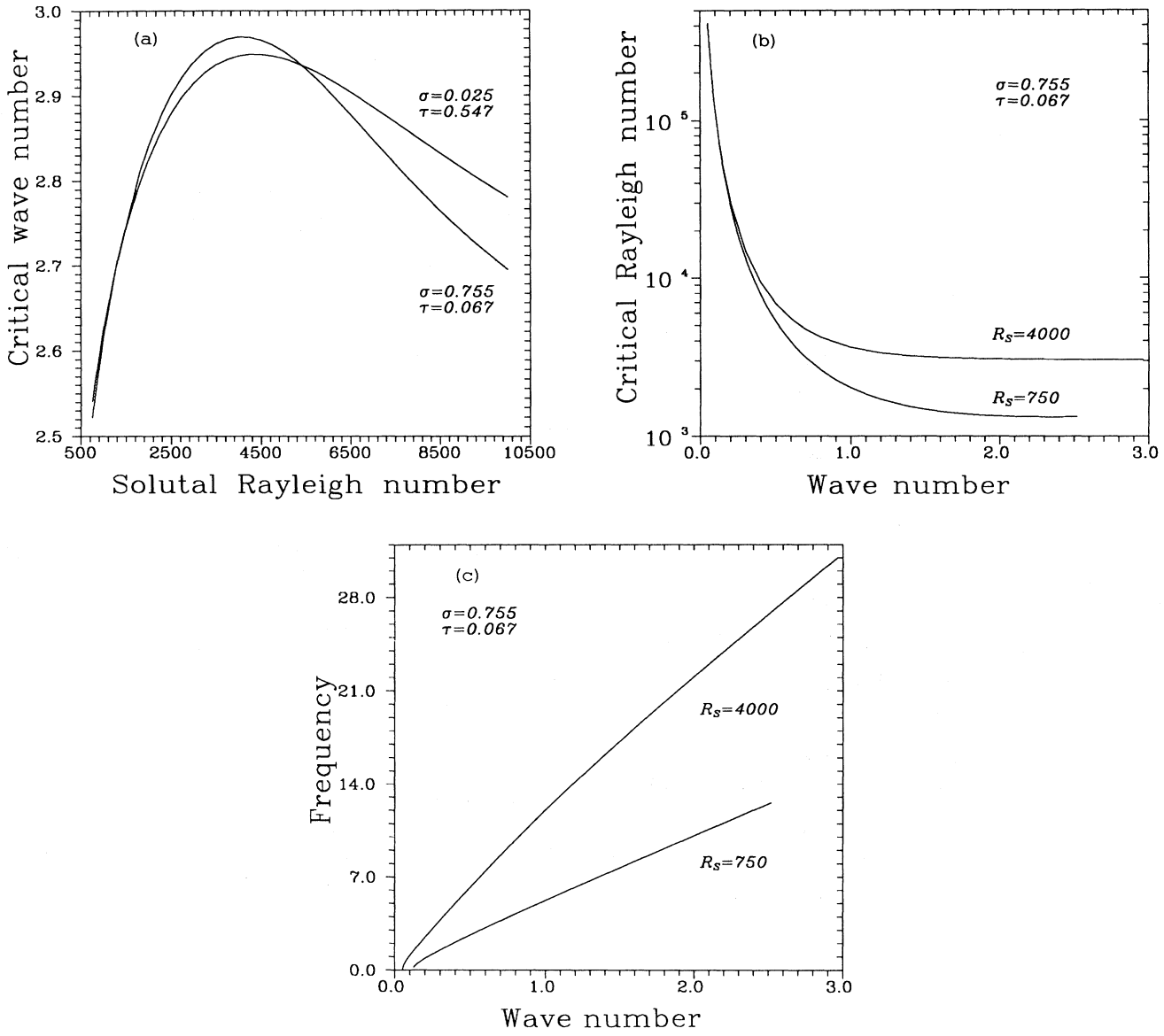

FIG. 8. (a) The upper bounds m_c^+ for the existence of wall modes as a function of R_S for $\tau = 0.067$, $\sigma = 0.755$, and for $\tau = 0.025$, $\sigma = 0.547$. (b) R_{Tc} and (c) ω_c as functions of m, $m_c^- < m < m_c^+$, for $\tau = 0.067$, $\sigma = 0.755$, and R_S=750 and 4000. R_{Tc} reaches a minimum at m=2.34 and 2.86, respectively.

cutoff value of m continue to increase monotonically with R_S (not shown). As m decreases towards m_c^- the critical Rayleigh number for a wall mode increases dramatically [Fig. 8(b)]; a much weaker increase in R_{Tc} takes place as $m \to m_c^+$. For $R_S = 750$ the minimum value of R_{Tc} occurs at $m \equiv m_{\min} = 2.34$ and is $R_{Tc} = 1320.80$. The corresponding frequency is $\omega_c = 11.7$. In contrast, for $R_S = 4000$, $m_{\min} = 2.86$ and $R_{Tc} = 3058.26$, $\omega_c = 30.1$.

Although the above solutions cannot be directly compared with those presented in Fig. 5 on account of the different boundary conditions at the top and bottom and the finite aspect ratio of the system, they do provide a confirmation that wall modes can be present even in nonrotating systems provided only that the initial bifurcation is a Hopf bifurcation that breaks the azimuthal symmetry of the system. While we have not found parameter values for which such modes are the ones that first become unstable, it is clear that such a possibility must be allowed for in stability problems of this type. In particular, we expect that with rigid walls at top and bottom the critical Rayleigh number for the body modes will be raised more than that for the wall modes. Consequently, such wall modes are most likely to be observed precisely under the conditions prevailing in experiments. In this connection we note that the parameter values listed above for Fig. 7 correspond to the following values

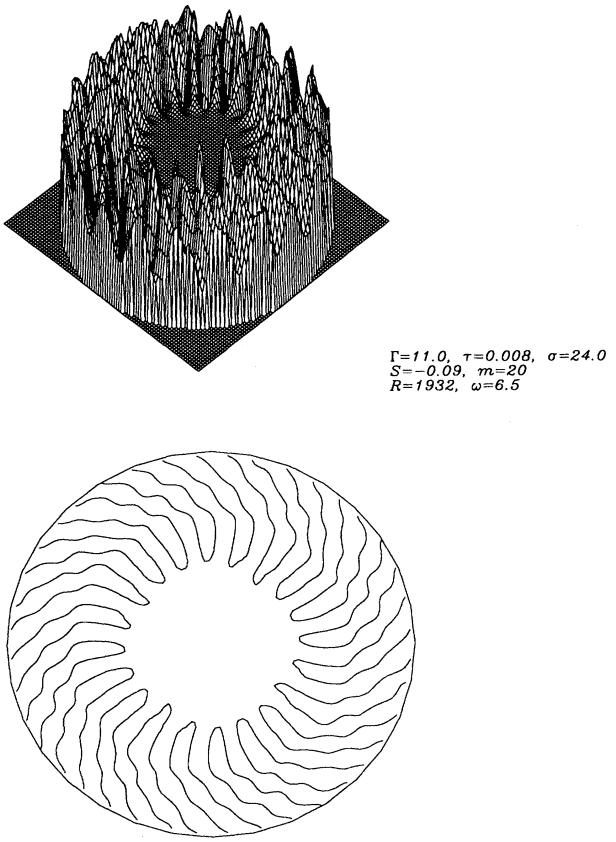

FIG. 9. An $m = 20$ wall mode in a $\Gamma = 11.0$ container with $\tau = 0.008$, $\sigma = 24.0$, $S = -0.09$, and rigid boundaries. For this mode $R_c^{(20)} = 1932$ and $\omega_c^{(20)} = 6.5$. Note that $R_c^{(20)}$ is only slightly larger than $R_c^{(1)}$; cf. Fig. 6.

in the equivalent Soret problem [22]: (a) $R_c^{(1)} = 1972.85$, $S = -0.3547$ ($m = 1$), $R_c^{(2)} = 1288.19$, $S = -0.5432$ ($m = 2$); (b) $R_c^{(1)} = 2733.49$, $S = -0.2502$ ($m = 1$), $R_c^{(2)} = 1693.19$, $S = -0.4040$ ($m = 2$). Note in particular that the minimum Rayleigh number wall mode corresponds approximately to an azimuthal wave number $\Gamma m_{\min}$ in a cylinder of (large) aspect ratio Γ. For the parameter values used this gives $m \approx 26$ for the $\Gamma = 11$ cell used by Lerman *et al.* [1] with $R_c = 1270.55$, $S = -0.5507$. Such modes would therefore appear entirely different from the body modes described so far. They would have high azimuthal wave number and be confined closely to the vicinity of the wall (see Fig. 9), in contrast to the body modes (see Fig. 6).

VI. DISCUSSION

In this paper we have presented sample results characterizing the onset of the oscillatory instability in binary fluids with a negative separation ratio confined to a vertical cylinder. We have found eigenfunctions in the form of clockwise or counterclockwise rotating spirals. As in the corresponding pure fluid problem in a rotating cylinder, the modes can be of two types, either spatially extended body modes or wall modes confined to the outer wall of the cylinder. For the parameter values examined a body mode is always the first mode that becomes unstable. In general, the mode structure of the present problem is unquestionably of comparable complexity to that found for a pure fluid in a rotating cylinder [10, 23]. Although we have chosen here not to dwell on this complexity, we emphasize that there is in general a number of families of both wall and body modes which change their dominance as parameters are varied, much as in the rotating problem. In particular, our calculations indicate the presence for $m > m_c^+$ of other families of wall modes, although with higher Rayleigh numbers. The results presented here have focused on the dominant family for the assumed parameter values, with the higher lying modes omitted.

Experiments on binary fluid convection in a vertical cylinder have been reported by a number of authors. These include experiments of Lee *et al.* [24] and Gao and Behringer [25] using normal ^{3}He-^{4}He mixtures (see also Refs. [26] and [27]) and by Rosenberger *et al.* [28] using gaseous Xe-He, Xe-Ar, and $SiCl_4$-H_2 mixtures with positive separation ratios. The calculations of the present paper were motivated by ongoing experiments on mixtures with negative separation ratios, and in particular those of Lucas and co-workers [12] on ^{3}He-^{4}He mixtures in a *rotating* cylinder, and by Lerman *et al.* [1] on water-ethanol mixtures in a nonrotating cylinder. These in turn motivated our choice of parameters. It should be noted that several of the cryogenic experiments in which direct flow visualization was impossible failed to report the presence of oscillations for the separation ratios for which theory predicts the onset of convection via a Hopf bifurcation [24, 25, 27]. We believe that this is because the instability evolves into azimuthally propagating waves of fixed form which transport a constant amount of heat, i.e., produce a time-independent Nusselt number (cf. [3, 16]). As a result we cannot compare the theoretically predicted frequencies ω_c with data; for these experiments the comparison is thus limited to the critical Rayleigh numbers. The measured Rayleigh number cannot usually be used to deduce the azimuthal wave number of the instability because for moderate to large aspect ratios the curves of $R_c^{(m)}(S)$ fall very close to one another. On the other hand, predictions of the onset azimuthal wave number have been tested for pure fluids in a rotating cylinder [10] and found to agree well with the experiments for which visualization was possible [15]. Thus we believe that the theory predicts reliably not only critical Rayleigh numbers and frequencies at onset, but also the azimuthal wave number of the instability.

Lerman *et al.* [1] investigated water-ethanol mixtures with $\Gamma = 11.6$ and $S = -0.09$, -0.10, -0.14, and -0.16. In each case the onset state appeared to consist of growing waves propagating in the radial direction. In subsequent experiments, with $\Gamma = 11.0$, $\tau = 0.008$, and $\sigma = 24$ the initial instability is to an $m = 1$ mode that propagates predominantly in the radial direction. These obser-

vations can be compared with the results shown in Fig. 6 which show an $m = 1$ eigenfunction for the experimental parameter values. The eigenfunction takes the form of a spiral (either left handed or right handed) consisting of outward propagating nodes together with azimuthal drift. For this mode $R_c^{(1)} = 1916.8$, $\omega_c^{(1)} = 6.16$, and the eigenfunction is strictly periodic, with period $2\pi/\omega_c^{(1)}$. For $m = 3$ (not shown) the results are similar. Here $R_c^{(3)} = 1917.2$, $\omega_c^{(3)} = 6.14$. Other m values, including $m = 0$ and $m = 2$, have larger critical Rayleigh numbers; all the critical Rayleigh numbers are close to one another, however, because of the large aspect ratio. Consequently it comes as no surprise that in the experiment an $m = 1$ mode can be contaminated by an $m = 3$ mode, as observed [29].

An immediate consequence of the general theory of the Hopf bifurcation with O(2) symmetry is the presence of finite amplitude spiral wave solutions to the full nonlinear equations describing binary fluid convection in a circular container. This solution bifurcates from the conduction solution at the Hopf bifurcation together with a standing wave state composed of an equal amplitude superposition of left-handed and right-handed spirals. The theory indicates that at most one of these branches can be stable. Spiral wave states are of course well known in reaction-diffusion systems, but have only recently been observed in fully three-dimensional systems like convection [30]. In the present system the experiments of Lerman *et al.* [1] indicate that the resulting steadily precessing nonlinear spiral is in fact unstable to modulational instabilities. We surmise that this is the case because the spirals in fact bifurcate subcritically by analogy with the corresponding situation in two dimensions. The possibility remains that when the two-dimensional traveling waves bifurcate supercritically (for values of S near the codimension-2 value [31]) the corresponding spirals will also bifurcate supercritically, and hence could be stable.

ACKNOWLEDGMENTS

We are grateful to G. Ahlers, S. Friedlander, K. Lerman, and P. Lucas for helpful discussions. The work of I.M. and M.N. was supported by the Fundació Catalana per a la Recerca and that of E.K. was supported by an INCOR grant from Los Alamos National Laboratory.

[1] K. Lerman, E. Bodenschatz, D. S. Cannell, and G. Ahlers, Phys. Rev. Lett. **70**, 3572 (1993).
[2] D. Bensimon, P. Kolodner, C. M. Surko, H. Williams, and V. Croquette, J. Fluid Mech. **217**, 441 (1990).
[3] E. Knobloch, Phys. Rev. A **34**, 1538 (1986).
[4] H. Riecke, Phys. Rev. Lett. **68**, 301 (1992).
[5] J. D. Crawford and E. Knobloch, Annu. Rev. Fluid Mech. **23**, 341 (1991).
[6] P. Kolodner, C. M. Surko, and H. Williams, Physica D **37**, 319 (1989); V. Steinberg, J. Fineberg, E. Moses, and I. Rehberg, *ibid.* **37**, 359 (1989).
[7] G. Dangelmayr and E. Knobloch, Nonlinearity **4**, 399 (1991); G. Dangelmayr, E. Knobloch, and M. Wegelin, Europhys. Lett. **16**, 723 (1991).
[8] E. Knobloch and D. R. Moore, Phys. Rev. A **37**, 860 (1988).
[9] F. Marqués, I. Mercader, M. Net, and J. M. Massaguer, Comput. Appl. Mech. Eng. **110**, 157 (1993).
[10] H. F. Goldstein, E. Knobloch, I. Mercader, and M. Net, J. Fluid Mech. **248**, 583 (1993).
[11] G. R. Hardin, R. L. Sani, D. Henry, and B. Roux, Int. J. Num. Methods Fluids **10**, 79 (1990).
[12] P. G. J. Lucas, M. S. Thurlow, M. R. Ardron, J. K. Bhattacharjee, B. J. Kershaw, M. D. J. Terrett, and A. L. Woodcraft, Physica B **194-196**, 841 (1994); M. S. Thurlow, Ph.D. thesis, University of Manchester, 1993.
[13] The shielding of the codimension-2 point by steady state instabilities with a different wave number that takes place in unbounded systems (see Ref. [8]) does not occur in finite containers.
[14] F. Zhong, R. E. Ecke, and V. Steinberg, Physica D **51**, 596 (1991); R. E. Ecke, F. Zhong, and E. Knobloch, Europhys. Lett. **19**, 177 (1992).
[15] F. Zhong, R. E. Ecke, and V. Steinberg, J. Fluid Mech. **249**, 135 (1993).
[16] E. Knobloch, A. Deane, J. Toomre, and D. R. Moore, Contemp. Math. **56**, 203 (1986).
[17] A. E. Deane, E. Knobloch, and J. Toomre, Phys. Rev. A **36**, 2862 (1987).
[18] J. Herrmann and F. H. Busse, J. Fluid Mech. **255**, 183 (1993).
[19] E. Y. Kuo and M. C. Cross, Phys. Rev. E. **47**, R2245 (1993).
[20] S. Friedlander and W. L. Siegmann, J. Fluid Mech. **114**, 123 (1982).
[21] L. N. Da Costa, E. Knobloch, and N. O. Weiss, J. Fluid Mech. **109**, 25 (1981).
[22] This transformation is given by $R = R_T - \tau R_S$, $S = -(1-\tau)\left(\frac{R_T}{R_S} - \tau\right)^{-1}$. See E. Knobloch, Phys. Fluids **23**, 1918 (1980).
[23] H. F. Goldstein, E. Knobloch, I. Mercader, and M. Net, J. Fluid Mech. **262**, 293 (1994).
[24] G. W. T. Lee, P. Lucas, and A. Tyler, J. Fluid Mech. **135**, 235 (1983).
[25] H. Gao and R. P. Behringer, Phys. Rev. A **34**, 697 (1986).
[26] T. Onions, M. R. Ardron, P. G. J. Lucas, M. D. J. Terrett, and M. S. Thurlow, Physica B **165&166**, 521 (1990).
[27] T. J. Bloodworth, M. R. Ardron, J. K. Bhattacharjee, P. G. J. Lucas, and N. D. Stein, Nonlinearity **3**, 981 (1990).
[28] J. M. Olson and F. Rosenberger, J. Fluid Mech. **92**, 631 (1979); J. R. Abernathey and F. Rosenberger, Phys. Fluids **24**, 377 (1981).
[29] K. Lerman and G. Ahlers (private communication).
[30] E. Bodenschatz, J. R. de Bruyn, G. Ahlers, and D. S. Cannell, Phys. Rev. Lett. **67**, 3078 (1993); S.W. Morris, E. Bodenschatz, D. S. Cannell, and G. Ahlers, *ibid.* **71**, 2026 (1993); M. Assenheimer and V. Steinberg, Nature **367**, 345 (1994).
[31] W. Schöpf and W. Zimmermann, Europhys. Lett. **8**, 41 (1989); T. Clune and E. Knobloch, Physica D **61**, 106 (1992).